The effect of composition and microstructure on the creep behaviour of 14 Cr ODS steels consolidated by SPS

Meza, A.; Macía, E.; Chekhonin, P.; Altstadt, E.; Rabanal, M. E.; Torralba, J. M.; Campos, M.;

Originally published:

June 2022

Materials Science and Engineering A 849(2022), 143441

DOI: https://doi.org/10.1016/j.msea.2022.143441

The effect of composition and microstructure on the creep behaviour of 14 Cr ODS steels consolidated by SPS

A. Meza[1,2], E. Macía[3], P. Chekhonin[4], E. Altstadt[4], M.E. Rabanal[2], J.M. Torralba[1,2], M. Campos[2]

[1] *IMDEA Materials Institute, Eric Kandel, 2, 28906 Getafe, Madrid, Spain, juanalberto.meza@imdea.org, josemanuel.torralba@imdea.org*

[2] *Univ. Carlos III of Madrid & IAAB, Av. Univ. 30, 28911 Leganés, Madrid, Spain juanalberto.meza@uc3m.es, eric.macia@uc3m.es*, mariaeugenia.rabanal@uc3m.es, monica.campos@uc3m.es*

[4] *Helmholtz-Zentrum Dresden-Rossendorf (HZDR), Bautzner Landstraße 400, 01328 Dresden, Germany p.chekhonin@hzdr.de, e.altstadt@hzdr.de*

ABSTRACT

There is a general need for alternative structural materials to improve power plants' efficiency and reduce CO_2 emissions. Within this framework, two new compositions of temperature-resistant sintered ODS ferritic steels (14Cr-5Al-3W), strengthened by a fine dispersion of precipitates ($5 \cdot 10^{22}$ ox. /m^3), have been developed. This work focuses on creep properties and microstructure evolution. The creep resistance (at 650°C) could be improved by prior microstructural optimisation, thanks to the consolidation by spark plasma sintering and the tailoring of precipitates' nature when a single compound introduces the oxide-forming elements (Y-Ti-Zr-O) synthesised for this purpose. To this end, the initial pre-alloyed ferritic powder was mechanically alloyed with the synthesised compound and sintered by spark plasma sintering (SPS). Afterwards, EBSD and TEM characterisation were employed to study the microstructures. Small punch creep tests (SPCT) were performed on the steels to analyse their creep performance. These showed an exceptional enhancement of the creep resistance in the steels containing the Y-Ti-Zr-O additions.

Keywords: 14Cr-ODS steel, fine grain, creep behaviour, SPCT

1. INTRODUCTION

High-efficiency power plants and the Gen. IV nuclear reactors are called to meet the ongoing energetic demand. Hence, the structural materials conforming these power plants must be excellent regarding security and thermal efficiency. The oxide dispersion strengthened (ODS) ferritic steels (FS) are valid candidates for these applications thanks to their fair distribution of nanometric oxides, which confer a notable mechanical behaviour at room and high temperatures. The oxides act as pinning points to the movement of the dislocations and the grain boundaries while providing irradiation resistance to the steels as they act as sinks for vacancies and other defects.

Nevertheless, the creep phenomenon is an essential factor to consider, as it usually appears in the environments in which these steels must work. Thus, it is imperative to develop ODS FS with microstructures that grant an enhanced creep resistance and for that, selecting the adequate composition and processing is fundamental.

In terms of composition, chromium and aluminium can provide proper oxidation and corrosion resistance to the steels, besides maintaining 14 wt.% Cr ensures their ferritic (BCC) microstructure. Adding tungsten to the steel deliver solid solution strengthening, especially at high temperatures (HT) [1]. For the dispersion of fine oxides, traditionally, yttrium oxide (Y_2O_3) has been used in conjunction with titanium (as oxide former), which is also responsible for the refinement of the oxides [2,3]; however, despite the presence of Ti, in Al-containing ODS steels,

*Dr. E. Macía corporation's email: eric.macia@acerinox.com

Y-Al-O type oxides form as coarse oxides that due to their nature and coherency do not reinforce the steels by precipitation strengthening as effectively, hence, the inclusion of zirconium helps in this matter as it promotes the precipitation of fine Y-Zr-O oxides and further refines and improves the oxides densities within the ODS FS [4]. Furthermore, including the oxide forming' elements (Y, Ti, Zr) as a whole unique compound can improve the precipitation of the oxides. Thus, enriched environments containing these elements will be produced and will develop more refined and distributed nanometric oxides [5].

Concerning the processing of these ODS FS, the powder metallurgy (PM) route provides various benefits. It involves more precise control of the final composition of the manufactured alloys, which in turn, gives rise to the attainment of microstructures that can equal or surpass the creep behaviour of other commercial ODS steels from the literature that, on the other hand, were developed through more complex routes that implicate additional processing stages than the one chosen in this investigation. Thus, competitive high-performance ODS FS were processed in this work by obtaining the powders through mechanical alloying (MA) followed by a spark plasma sintering (SPS) consolidation, providing the steels with a superior precipitates' strengthening that limits the formation of coarse Y-Al-O oxides. Furthermore, because SPS is an activated sintering process, grain growth will also be inhibited. Altogether, tailoring the steels' microstructure could adequately withstand the creep phenomena and make them valid candidates for their application in powerplants, in which the creep process is typical.

In the end, the creep performance of the steels was studied through small punch creep tests (SPCT) that, although still a novelty in this field, gave in return critical information about the creep resistance and creep mechanisms in the steels. Lately, the SPCT has been attracting attention because of its ability to determine the creep properties of various metallic families using reduced amounts of material in contrast to the widely used uniaxial creep tests [6]. Thus, these tests are employed as an alternative approach to characterise the properties of the materials with small specimens. Hence, this work compares and discusses the differences in creep behaviour between the two new ODS FS compositions and another steel previously studied in the literature [7,8] as a reference.

2. EXPERIMENTAL PROCEDURE

The ODS steels compositions (**Table 1**) were manufactured from raw powders such as a pre-alloyed grade Fe-14Cr-5Al-3W (Sandvik Osprey Powder Group), highly pure Ti powder (GFE mbH, Nuremberg, Germany), Y_2O_3 powder (TJ Technologies & Materials Inc., Shanghai, China) and pure B powder (Good Fellow Cambridge); additionally, a complex-oxide nanometric powder (Y-Ti-Zr-O) containing all the oxides formers was synthesised as described in [5].

Table 1: *Composition (wt.%) of the processed ferritic ODS FS, the Y-Ti-Zr-O compound was synthesised at the lab, and its amount was set to maintain an addition of 0.6 wt.% Zr. In this research, 14Al-Ti-ODS was considered as reference steel.*

	Prealloyed (%)				***Oxide formers (%)***			***Other alloying elements (%)***
	Fe	***Cr***	***Al***	***W***	***Y_2O_3***	***Ti***	***Y-Ti-Zr-O***	***B***
14Al-Ti-ODS	*bal*	*14*	*5*	*3*	*0.25*	*0.4*	*-*	*-*
14Al-X-ODS	*bal*	*14*	*5*	*3*	*-*	*-*	*1.62*	*-*
14Al-X-ODS-B	*bal*	*14*	*5*	*3*	*-*	*-*	*1.97*	*0.1*

To obtain the powders of each composition, the mixtures of starting base powders were mechanically alloyed (MA) by high-energy milling using a horizontal ZOZ Attritor mill (Simoloyer

CM01 type) under a highly pure argon (Ar) atmosphere (99.9995 vol. %), running during all the processing time, once three purges were performed in the vacuum system. Balls of 5 mm diameter were used, keeping the ball-to-powder ratio at 20:1. The rotation speed was set at 800 rpm, with a final effective milling time of 40 h for all compositions, to induce an equivalent level of plastic deformation through mass collisions in the three obtained ODS ferritic steels.

The spark plasma sintering (SPS) technique was selected to consolidate and densify the milled powders while limiting the steels' grain growth. Samples were sintered using an SPS equipment FCT System GmbH. To avoid C contamination from the graphite dies, a high-purity (>99.97%) tungsten foil was used during the sintering process. Subsequently, the milled ODS powders were put into a 20 mm cylindrical graphite die and heated in a vacuum (10^{-2}-10^{-3} mbar). Parameters related to the consolidation are given in ***Table 2***.

Table 2: *SPS Consolidation parameters*

Parameter	
Sintering Temperature (°C)	*1100*
Heating rate (°C/min)	*400*
Pressure (MPa)	*80*
Holding time (s)	*300*

The microstructural characterisation of the processed ODS steels was developed for both the milled powders and the consolidated samples. SEM (FEI Teneo) was employed to study the powders' size and morphology. Furthermore, to analyse the crystallographic parameters involved in the MA, X-ray measurements were performed with X'Pert Phillips equipment using Cu_{α} radiation with a step size of 0.02 degrees and a step time of 2.4 s. These examinations estimated the crystallite size (L) and the microstrain values (με) through the Scherrer and the Williamson-Hall equations, respectively.

The sintered samples' relative density was measured from image analysis in several SEM images (FEI Teneo, 10000 μm^2 for each ODS). Their grain microstructure was examined through EBSD (Zeiss Ultra 55 Plus SEM equipped with a System Channel 5 EBSD detector). The grains in the transversal section of the consolidated samples were analysed using step sizes of 150 nm. The evaluation was done with an in-house written software (*P. Chekhonin*); a misorientation threshold angle of 5 degrees was used for grain separation. TEM investigations were carried out with FEI Talos F200x TEM equipment using STEM, HAADF, BF or WBDF modes to precisely determine the main features of the nanometric precipitates within the consolidated ODS steels as their size and distribution.

Microhardness measurements at room temperature were carried out in the non-ODS and the ODS steels with a load of 1.96 N using a Zwick Roell Microhardness equipment (by Indentec Hardness Testing Machines Limited, United Kingdom, UNE-EN ISO 6507-1:2006 standard). Samples were polished to achieve mirror-like surfaces.

The SPCT were carried out at the Helmhotz Zentrum Dresden-Rossendorf institute, in Dresden, Germany. The conditions used to perform the SPCT were the following: a temperature of 650 °C was selected, and different loads (250 N, 275 N, 300 N) were applied in circular/disk shape samples with a diameter of 8 mm and a thickness of 500 µm. The lower and upper die had a ring shape and were connected via a thread to hold the exterior of the specimen statically during the test so that only the central area of the disc specimen would deform due to the creep process. A ceramic punch ball applied the load in contact with the centre of the specimen. A plunger rod

was used to transmit a constant load to the punch ball. All these components were made of Al_2O_3. An electrical heater and thermal insulation surrounded the clamping device to ensure the temperature during the test. Pillars with ball-bearings guided the upper plate carrying the additional deadweight. The temperature was measured in the lower die directly under the sample. The displacement was measured by a capacitive sensor between the upper plate and the thermal insulation with an accuracy of ±1 µm. A load cell was placed between the upper plate and plunger rod. An electric spindle could lock the upper plate with the dead weight. This enabled the start of the loading on the sample after heating up and reaching the thermal equilibrium of the set-up. The experimental set-up was entirely covered by a sealed shell which was evacuated and flooded with Ar before the test. A schematic of the process is shown in **Figure 1**.

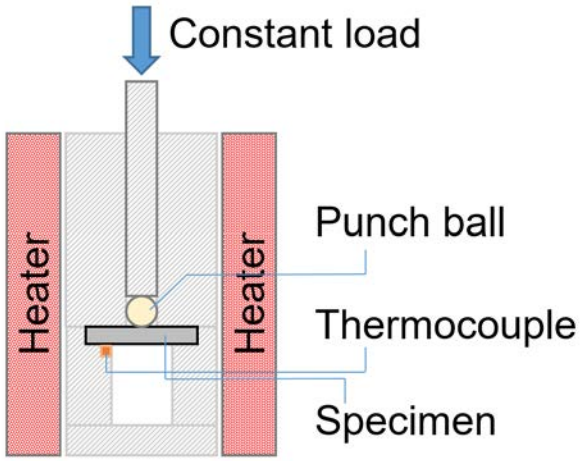

Figure 1: *Schematic of the SPCT equipment*

3. RESULTS

3.1. Consolidation of new ODS steels.

Figure 2 shows the changing morphology of the powders as the different processing stages took place. The spherical pre-alloyed powder became irregular after the MA due to the heavy plastic strain applied to them during the milling stage for 40 h.

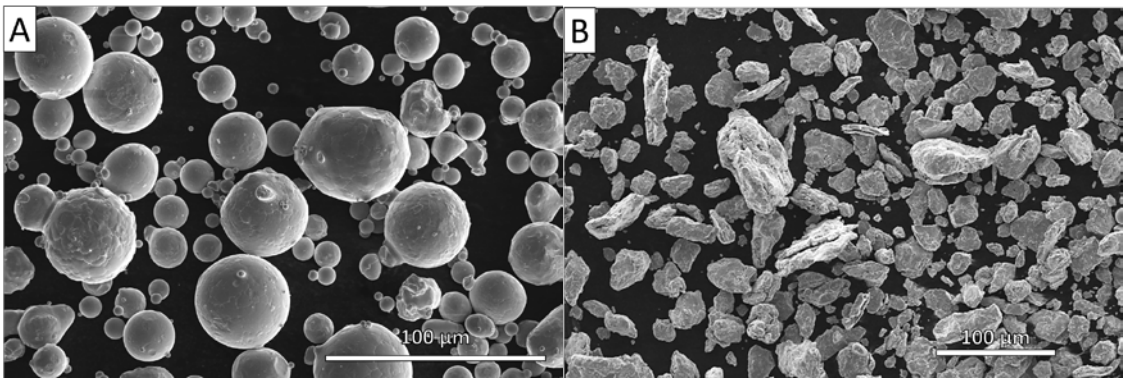

Figure 2: *SEM SE images of the steel powders: A) pre-alloyed powder, B) after MA for 40 h*

The MA step should reach a stationary state where both the cold-welding and fracture phenomena conclude into equilibrium. For that reason, the evolution of the crystallographic parameters was studied (**Figure 3**), precisely the powders' crystallite size (L) and microstrain

levels (με). A decrease of L and a rise of the με were noticed once the MA was developed due to a significant increase in the dislocations density, strengthening the powders.

Increasing the dislocations density in the powders is also an essential contribution to achieving adequate strengthening in the final ODS steels. It is necessary to limit the loss of dislocations during the consolidation stage, so methods that restrain diffusive phenomena but allow complete consolidation, e.g. SPS, must be chosen.

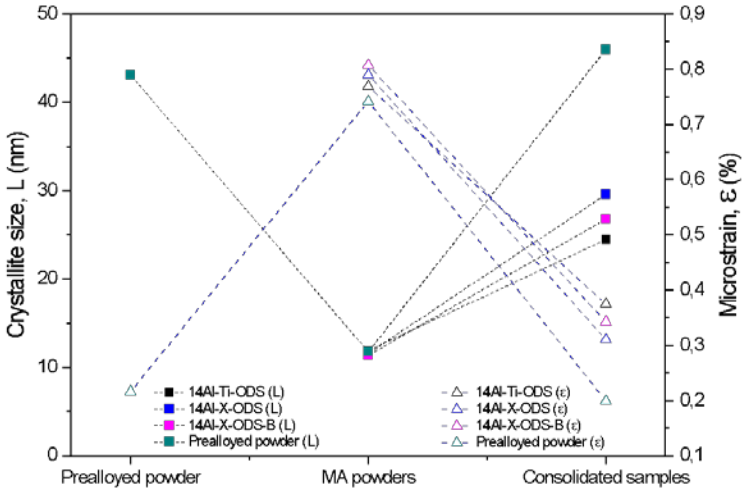

Figure 3: *Evolution of crystallite size (left axis, grey dotted line) and microstrain (right axis, blue segmented line) during manufacturing*

EBSD mappings were performed in the transversal section of the consolidated samples (***Figure 4***) to analyse grain size distribution, and no texture was observed. Thus, the grains did not grow in a preferential crystallographic direction during the SPS consolidation. Besides, a bimodal grain microstructure was recognised, as coarse grains (> 1 μm) areas surround smaller ultrafine (UF) grains (< 1 μm) colonies (**Table 3**).

Table 3: *Relative density and grain distribution of the processed ODS steels*

	Relative density (%)	***Mean size coarse grains (> 1 μm)***	***Mean size UF grains (< 1 μm)***	***UF area***
14Al-Ti-ODS	99.91 ± 0.01	3.03 μm	0.59 μm	5%
14Al-X-ODS	99.81 ± 0.01	2.48 μm	0.26 μm	13%
14Al-X-ODS-B	99.50 ± 0.02	2.83 μm	0.28 μm	16%

This bimodal grain distribution arose due to the elevated microstrain levels induced during MA and the pinning effect of the nanometric oxides. These factors promoted that each powder particle had different stored energy and, thus, a distinct ability to recrystallise. So they recovered and recrystallised dissimilarly during the consolidation process.

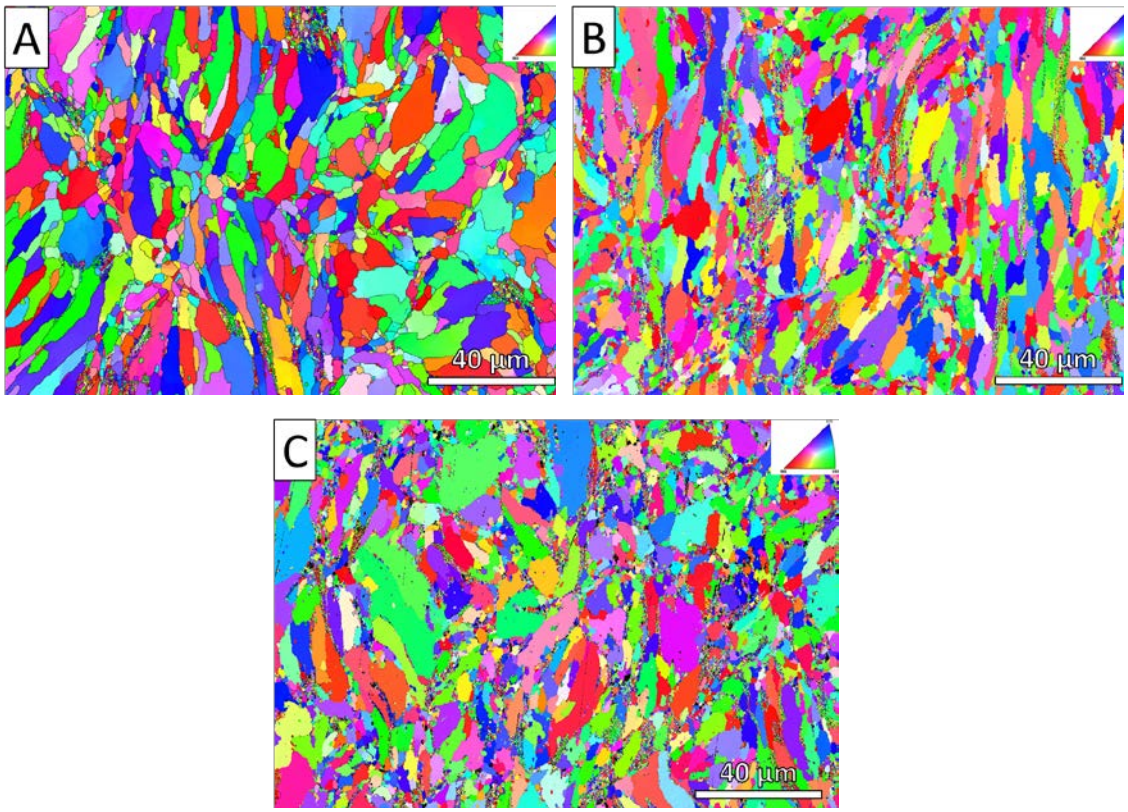

Figure 4: *EBSD IPF maps (sample normal direction) of the transversal section of consolidated steels: A) 14Al-Ti-ODS, B) 14Al-X-ODS, C) 14Al-X-ODS-B*

From the TEM micrographs, high dispersion of the nanometric oxides is observable (***Figure 5***).

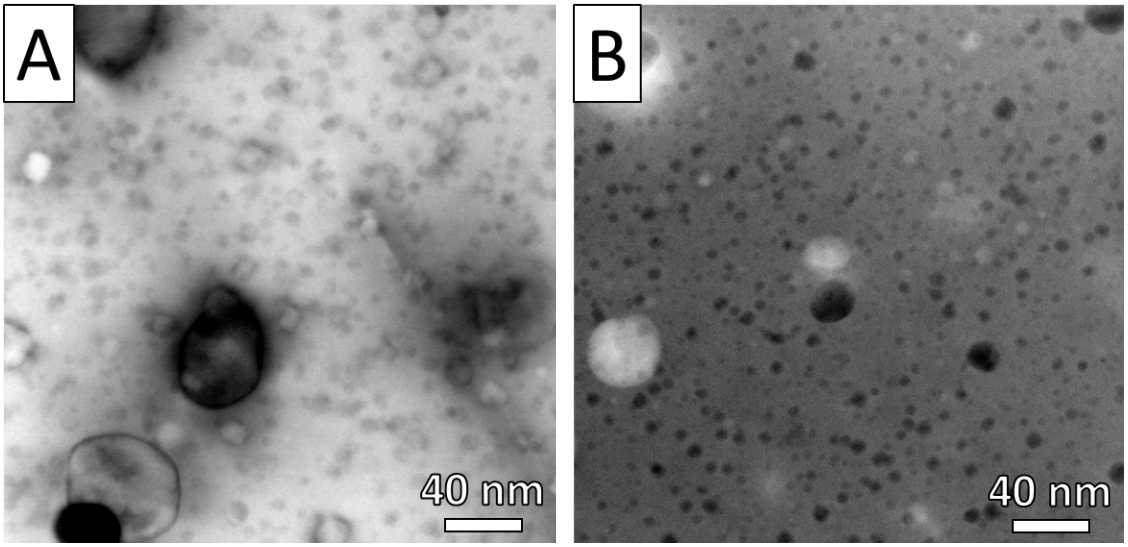

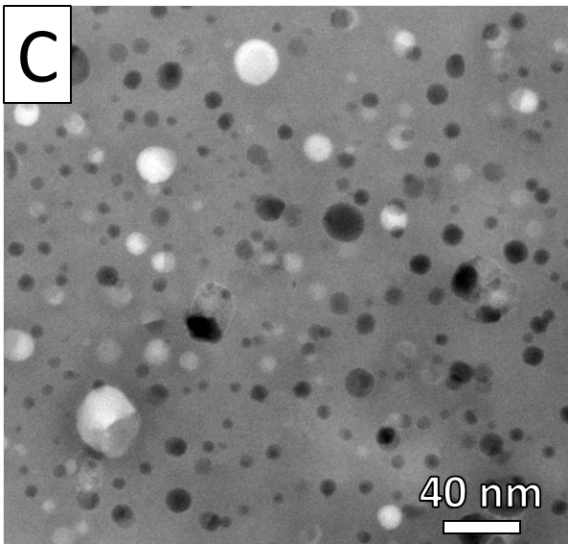

Figure 5: *STEM BF images of the precipitates in the ODS steels: A) 14Al-Ti-ODS, B) 14Al-X-ODS, C) 14Al-X-ODS-B*

The precipitates' sizes and densities of the ODS steels were calculated and compared in ***Table 4***. A decrease in the precipitates' size and an improvement in the density were notable when the Y-Ti-Zr-O was added. This happened due to the inclusion of Zr, which was inherent in the complex compound; this element could refine the precipitates by partially avoiding the formation of Y-Al-O oxides type and precipitating Y-Zr-O nano-oxides with smaller diameters. The binding energy of Y-Zr-O is higher than that of Y-Al-O at the temperature these precipitates form during the consolidation in a Fe matrix [4,9]. Hence, the establishment of Zr-containing precipitates is favoured over the Al-containing ones, resulting in a decrease in the overall average size of the nano-precipitates. Likewise, the precipitates' density rose due to the higher amount of oxides' formers in the steels with Y-Ti-Zr-O. These features could lead to the steels' enhanced mechanical and creep behaviour. More information concerning the composition of the precipitates in these steels can be found in [5].

Table 4: *Precipitates' sizes and densities for each processed ODS steel composition*

	Oxides' formers wt. %	***Average precipitates' size (nm)***	***Precipitates' density (precipitates/m^3)***
14Al-Ti-ODS	0.60	9.80 ± 0.03	$2.37 \cdot 10^{22}$
14Al-X-ODS	1.20	5.90 ± 0.04	$5.48 \cdot 10^{22}$
14Al-X-ODS-B	1.44	8.14 ± 0.01	$5.17 \cdot 10^{22}$

3.2. Mechanical and creep behaviour

When comparing the microhardness measurements at RT of the steels (***Figure 6***), it is evident how the inclusion of the oxides in the steels increased the hardness. Furthermore, a significant increase was observed in the ODS steels containing the complex oxide Y-Ti-Zr-O with respect to the reference composition (14Al-Ti-ODS) due the higher precipitates' densities achieved.

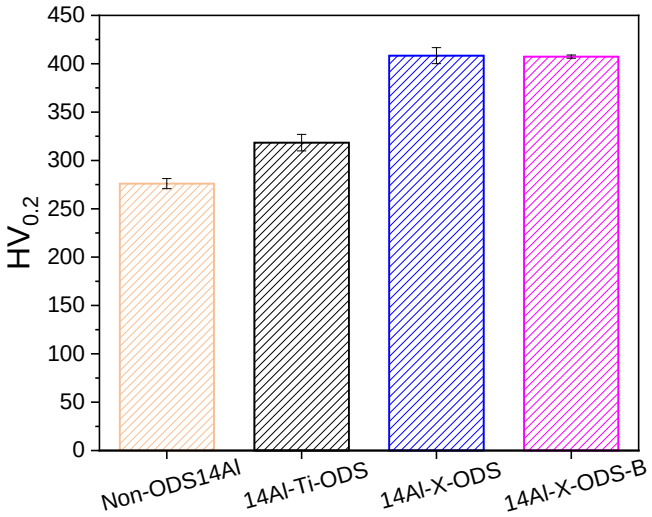

Figure 6: *Microhardness measurements of the processed ODS steels compared with the steel without ODS*

The creep curves obtained after the SPCT were represented in ***Figure 7***, and the main results extracted from them were compiled in ***Table 5***. Three main stages were identified in the creep curves: in the primary stage, the strain increased with time, decreasing the strain rate simultaneously. This can be explained due to the creation of new dislocations that ultimately diminished the movement of the dislocations. Once the new dislocations induced by the applied load were compensated by the annealing and recrystallisation processes of other dislocations due to the elevated temperature of the system, the strain rate remained constant; this behaviour is typical of the steady-state creep stage. Finally, in the tertiary stage, due to the appearance of necking and stretching of the membrane, the strain rate accelerated and ultimately led to the creep failure of the specimens.

Due to the bending deformation inherent in the SPC test, the curves' primary stages are usually sharper than conventional uniaxial creep curves. As in typical creep curves, the primary deflection stage and the continual deflection rate stage are reduced at a constant temperature and as the applied load increases. In addition, the rupture time also alters significantly by increasing the applied force.

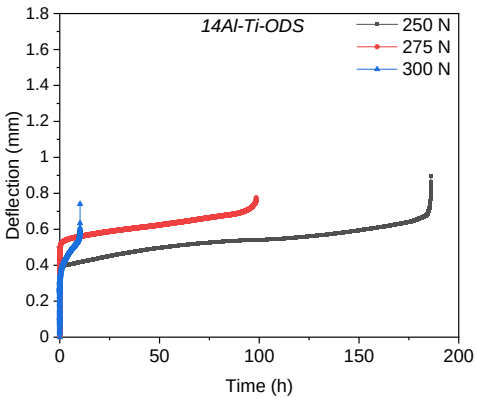

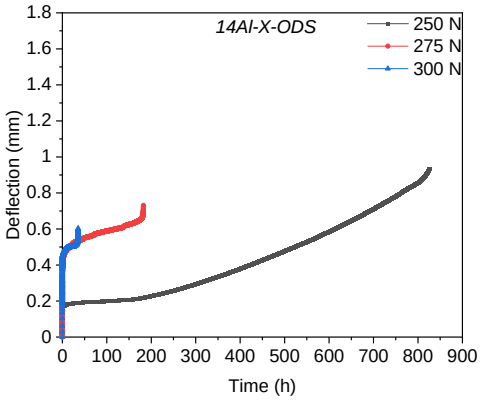

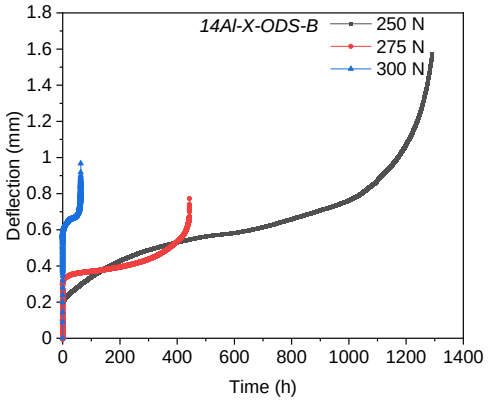

Figure 7: *SPCT creep curves of the ODS steels at 650 °C and different loads: 250 N, 275 N, 300 N*

The ODS compositions containing the complex compound Y-Ti-Zr-O and boron (14Al-X-ODS and 14Al-X-ODS-B) exhibited improved creep resistance regarding the reference ODS steel. The increase of the precipitates' density and the enhanced ratio of micrometric and UF grains when the Y-Ti-Zr-O was included were the main reasons for this enhancement of the creep behaviour.

Therefore, the effect of this addition was positive in enhancing their behaviour against creep. This fact was likewise supported by the lower minimum deflection rates and the higher times to rupture observed in the Y-Ti-Zr-O-containing ODS steels by comparing them with the reference material 14Al-Ti-ODS; the change in these values can be translated as a higher creep resistance of these steels.

Table 5: *Small punch creep results of the tested samples at 650 °C and different loads*

	Minimum disk deflection rate (µm/h)			**Time to rupture (h)**		
	250 N	**275 N**	**300 N**	**250 N**	**275 N**	**300 N**
14Al-Ti-ODS	0.3	1.3	2.3	186.0	98.4	10.2
14Al-X-ODS	0.1	0.5	0.3	826.2	182.5	35.5
14Al-X-ODS-B	0.2	0.2	0.5	1314.1	443.8	63.2

The creep behaviour in the processed ODS steels proved to be very satisfactory, especially the 14Al-X-ODS and 14Al-X-ODS-B ODS steel compositions when their performance was contrasted with other published investigations where comparable test conditions were applied to materials developed for similar applications. Experiments in P92 steel (a martensitic 9 wt.% Cr steel) also using the SPCT developed by *Zhao et al.* [10] have obtained reduced creep values (280 h being the longest rupture time) when matched to the ones obtained with the steels of this investigation. In other studies on G91 steel (9wt.%Cr) with a specially modified microstructure to improve creep response by incorporating MX carbides and thermomechanical treatments, *Vivas et al.* [11] have shown that under the most extreme test conditions, the maximum time to rupture has not exceeded 150 hours. It can be noted how the developed ODS FS in this work have surpassed these results. Furthermore, comparing the manufactured Y-Ti-Zr-O-added steels from this investigation with other commercial ODS steels such as the MA956 (ferritic 20 wt.% Cr steel reinforced with Y_2O_3 nano-oxides) or the GETMAT steel (14 wt.% Cr, MA, extruded and

containing Y_2O_3 nanoparticles) showed an improvement in the creep time to rupture; (see the analysis developed by *Bruchhausen et al.* in [12]).

To deepen the creep properties of the ODS steels tested by SPCT, an additional discussion was performed considering the relations between the minimum creep rate, the applied loads, and the time to rupture. In ***Figure 8, left***, the minimum deflection rate was represented against the applied load in the SPCT performed at 650 °C. Again, the comparison between the reference ODS steel (14Al-Ti-ODS) with the Y-Ti-Zr-O-added ODS steels (14Al-X-ODS and 14Al-X-ODS-B) showed how these last steels exhibited lower deflection rates, displaying their better resistance against creep. This reveals the effectivity of the precipitates at pinning the dislocations' movement inside the steels, especially the ones derived from the Y-Ti-Zr-O that reduced the minimum deflection rates more actively and thus, developed in longer times to rupture. This fact was confirmed in ***Figure 8, right***, where the load was outlined with the fracture times. It was proved how the retard on the onset of the tertiary creep state due to the interactions between dislocations and nano-oxides provoked the increase in the times to rupture.

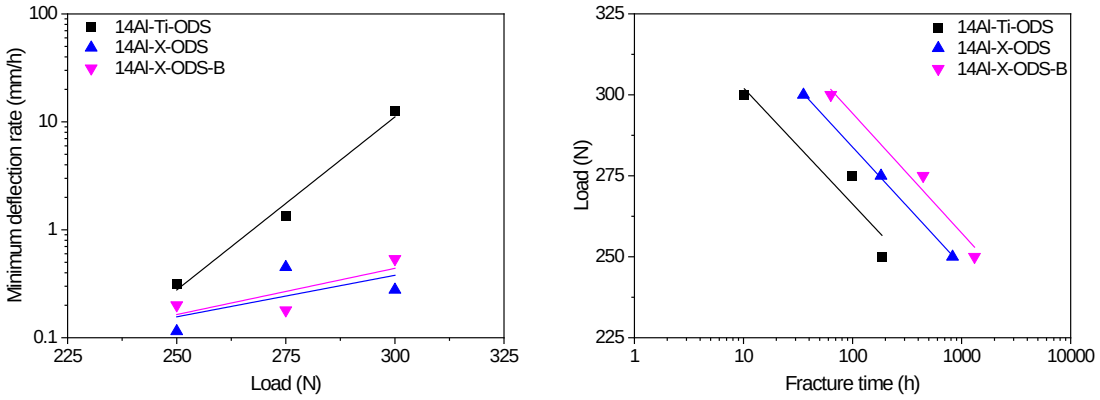

Figure 8: *Stress dependence of minimum creep rate at 650 °C for the developed ODS steels (left), load vs time to rupture of the processed ODS steels at 650 °C (right)*

Additionally, to define the predominant creep mechanism involved during the creep process, it is necessary to calculate the so-called Norton stress exponent (n), which establishes this mechanism by correlating the applied load during the SPCT with the minimum deflexion rate in Norton's law (***Eq. 1***).

$$\delta_d = A \cdot L^n \qquad (\textbf{Eq. 1})$$

Where δ_d is the minimum deflexion rate, A is the Temperature-dependent constant, L is the applied load, and n is the Norton exponent. Rewriting Norton's law (***Eq. 2***), it is possible to calculate this exponent through linear regression.

$$ln\left(\frac{\delta_d}{\delta_{250}}\right) = ln\left(\frac{A(T)}{\delta_{250}}\right) + n \cdot ln(L) \qquad (\textbf{Eq. 2})$$

In this equation, δ_{250} is referred to the minimum deflexion rate of the samples tested with the lower applied load in the SPCT, which in this work was equal to 250 N. Representing these natural logarithms of the load and the deflexion rates, the n stress exponent has been obtained as the slope of these lines, hence, providing information about the creep mechanisms associated with this exponent (***Figure 9***).

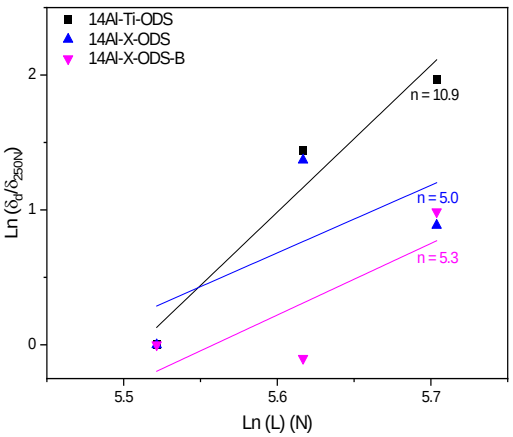

Figure 9: *Assessment of Norton's stress exponent (n) in the ODS steels*

The ODS steels containing the Y-Ti-Zr-O compound (14Al-X-ODS and 14Al-X-ODS-B) exhibited n stress exponents close to 5, which meant that the predominant creep mechanism activated was the dislocation climb-glide creep; that is, the value of 5 implied that the creep was mainly motivated by the interactions that took place between the dislocations and the precipitates [13]. Some scattering in these calculations is observed and it could be due to the effect of the bimodal and heterogeneous grain size distribution, as some of the small tested samples may have exhibited higher or lower grain sizes and so their associated Norton exponent varied. Future small punch creep tests developed in similar conditions may decrease this scattering. Nonetheless, acknowledging that the Norton exponent is usually employed in characterising samples tested by uniaxial creep tests is relevant [24,25]; in these tests, the samples are stretched with homogeneous stress. In the SPCT, this equivalent stress varies as the deflection in the samples increases, so the n stress exponents obtained with the SPCT may not be the same as the ones obtained with the uniaxial creep tests. Nevertheless, it has been meaningful to study this Norton's exponent in the SPCT performed in this work.

Finally, the Larson-Miller Parameter was calculated for the tested ODS steels in ***Figure 10***. A value of 30 was selected for the constant C in the LMP calculations, which is in accordance with other works from the literature in which the creep properties are analysed in ODS steels [12,14]. The 14Al-X-ODS and 14Al-X-ODS-B present a significantly improved creep lifetime than the reference ODS steel (14Al-Ti-ODS) at 650 °C. Furthermore, when these LMP-related creep results are compared with other works that follow similar methodology from the literature like [15,16], it is evident how, although all the studied materials are heat-resistant steels, the ones developed in this investigation exhibit superior creep resistance.

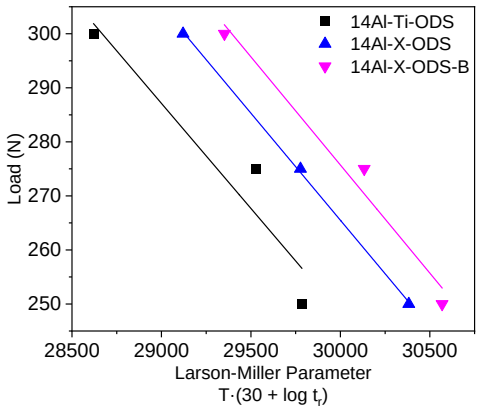

Figure 10: *Dependence of load on Larson-Miller Parameter of the processed ODS steels*

Focusing on the fracture mode of the tested samples, ***Figure 11*** shows the samples tested with a load of 300 N and at 650 °C. From the fractography analyses, the steels Y-Ti-Zr-O show some dimples and deformed necks, proving their ductility before breaking. Furthermore, during the SPCT, two strain modes have occurred, the bending of the membrane and the stretching of the same. The first deformation mode of bending has been associated with the primary stage of the creep regime. In contrast, the stretching of the membrane takes place during the secondary and tertiary stages [17].

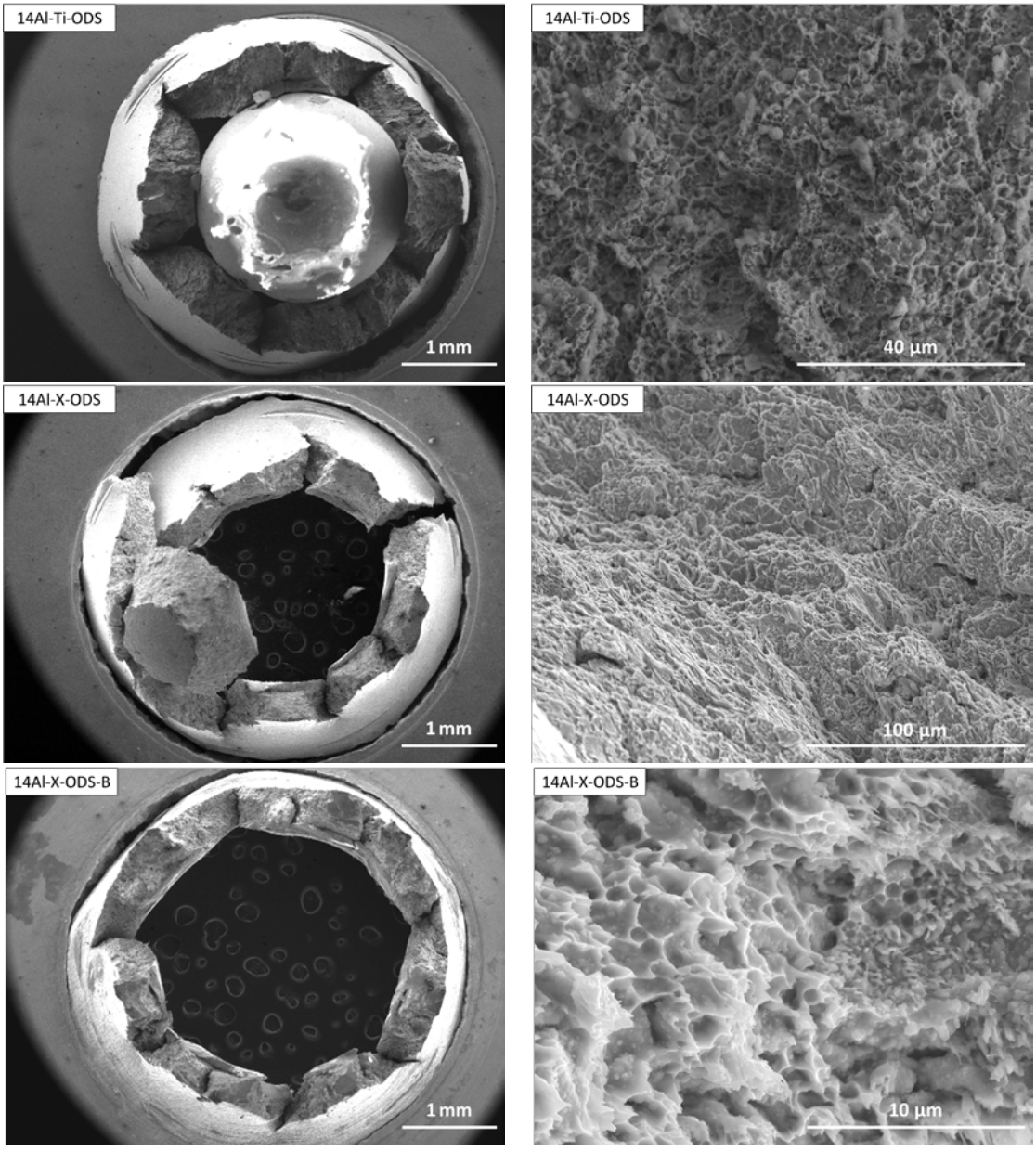

Figure 11: *Fracture images of the tested samples by SPCT with a load of 300 N at 650°C*

4. CONCLUSIONS

This research studied two ODS FS developed by PM in terms of microstructure and creep performance, varying their oxides' formers additions. The steels were processed using MA to obtain the initial powders, followed by an SPS consolidation. It was determined that:

- The selected parameters in the steels' manufacturing were favourable to achieving microstructures that deliver competitive ODS steels. The MA strengthened and homogenised the powders properly, while the SPS consolidated the steels at nearly-full densifications avoiding excessive grain growth simultaneously.
- The consolidated samples exhibited a bimodal grain microstructure composed of coarse-grain regions in conjunction with UF grain areas.
- The inclusion of the Y-Ti-Zr-O positively affected the obtained microstructures, as it was able to refine the grain size at both coarse and UF grain levels. It increased the formation of more extended UF grain areas. Furthermore, it enhanced the precipitation of the nanometric oxides attaining more refined oxides and at higher densities.
- The improved microstructures obtained by adding the Y-Ti-Zr-O complex compound revealed an exceptional creep performance on the ODS steels. The diminishing of their secondary deflection rates and the impressive increase in their times to rupture show the excellent creep behaviour of these compared with other candidate steels from the literature.
- The predominant creep mechanism involved in the ODS steels was the climb glide creep, which is promoted by the interactions between the inner dislocations and the nanometric precipitates.
- Overall, high-performance ODS FS was developed using a PM route that saved processing stages while achieving similar or better creep performance than other ODS steels.

Acknowledgements:

The authors want to acknowledge the Ferro-Ness project, Ferro-Genesys, and AFORMAR project for their funding by MINECO under the National I+D+I program MAT2016-80875-C3-3-R and PID2019-109334RB-C32. Additionally, acknowledgements to M. Houska from the HZDR institute for his help during the SPCT.

Data availability:

The raw data required to reproduce these findings are available and can be used prior authorisation from the authors. Contact *juanalberto.meza@imdea.org* for more information.

Bibliography:

[1] T. Narita, S. Ukai, S. Ohtsuka, M. Inoue, Effect of tungsten addition on microstructure and high temperature strength of 9CrODS ferritic steel, J. Nucl. Mater. 417 (2011) 158–161. https://doi.org/10.1016/J.JNUCMAT.2011.01.060.

[2] X. Boulnat, M. Perez, D. Fabrègue, S. Cazottes, Y. De Carlan, Characterisation and modeling of oxides precipitation in ferritic steels during fast non-isothermal consolidation, Acta Mater. 107 (2016) 390–403. https://doi.org/10.1016/j.actamat.2016.01.034.

[3] P. Dou, A. Kimura, R. Kasada, T. Okuda, M. Inoue, S. Ukai, S. Ohnuki, T. Fujisawa, F. Abe, Effects of titanium concentration and tungsten addition on the nano-mesoscopic structure of high-Cr oxide dispersion strengthened (ODS) ferritic steels, J. Nucl. Mater. 442 (2013) S95–S100. https://doi.org/10.1016/J.JNUCMAT.2013.04.090.

[4] J. Isselin, R. Kasada, A. Kimura, T. Okuda, M. Inoue, S. Ukai, S. Ohnuki, T. Fujisawa, F. Abe, Effects of Zr Addition on the Microstructure of 14%Cr4%Al ODS Ferritic Steels, Mater. Trans. 51 (2010) 1011–1015. https://doi.org/10.2320/matertrans.MBW200923.

[5] A. Meza, E. Macía, A. García-Junceda, L.A. Díaz, P. Chekhonin, E. Altstadt, M. Serrano, M.E. Rabanal, M. Campos, Development of new 14 Cr ODS steels by using new oxides formers and B as an inhibitor of the grain growth, Metals (Basel). 10 (2020) 1–16. https://doi.org/10.3390/met10101344.

[6] S. Arunkumar, Small Punch Creep Test: An Overview, Met. Mater. Int. 27 (2021) 1897–1914. https://doi.org/10.1007/s12540-020-00783-w.

[7] J.M. Torralba, L. Fuentes-Pacheco, N. García-Rodríguez, M. Campos, Development of high performance powder metallurgy steels by high-energy milling, Adv. Powder Technol. 24 (2013) 813–817. https://doi.org/10.1016/j.apt.2012.11.015.

[8] I. Hilger, X. Boulnat, J. Hoffmann, C. Testani, F. Bergner, Y. De Carlan, F. Ferraro, A. Ulbricht, Fabrication and characterisation of oxide dispersion strengthened (ODS) 14Cr steels consolidated by means of hot isostatic pressing, hot extrusion and spark plasma sintering, J. Nucl. Mater. 472 (2016) 206–214. https://doi.org/10.1016/j.jnucmat.2015.09.036.

[9] S. Mohan, G. Kaur, B.K. Panigrahi, C. David, G. Amarendra, Effect of Zr and Al addition on nanocluster formation in oxide dispersion strengthened steel - An ab initio study, J. Alloys Compd. 767 (2018) 122–130. https://doi.org/10.1016/j.jallcom.2018.07.047.

[10] L. Zhao, H. Jing, L. Xu, Y. Han, J. Xiu, Y. Qiao, Evaluating of creep property of distinct zones in P92 steel welded joint by small punch creep test, Mater. Des. 47 (2013) 677–686. https://doi.org/10.1016/j.matdes.2012.12.032.

[11] J. Vivas, C. Capdevila, E. Altstadt, M. Houska, M. Serrano, D. De-Castro, D. San-Martín, Effect of ausforming temperature on creep strength of G91 investigated by means of Small Punch Creep Tests, Mater. Sci. Eng. A. 728 (2018) 259–265. https://doi.org/10.1016/J.MSEA.2018.05.023.

[12] M. Bruchhausen, K. Turba, F. de Haan, P. Hähner, T. Austin, Y. de Carlan, Characterisation of a 14Cr ODS steel by means of small punch and uniaxial testing with regard to creep and fatigue at elevated temperatures, J. Nucl. Mater. 444 (2014) 283–291. https://doi.org/10.1016/J.JNUCMAT.2013.09.059.

[13] F. Abe, T.-U. Kern, R. Viswanathan, K. Maruyama, 8 - Fundamental aspects of creep deformation and deformation mechanism map, in: Creep-Resistant Steels, Woodhead Publishing, 2008: pp. 265–278.

[14] B. Fournier, A. Steckmeyer, A.L. Rouffie, J. Malaplate, J. Garnier, M. Ratti, P. Wident, L. Ziolek, I. Tournie, V. Rabeau, J.M. Gentzbittel, T. Kruml, I. Kubena, Mechanical behaviour of ferritic ODS steels – Temperature dependancy and anisotropy, J. Nucl. Mater. 430 (2012) 142–149. https://doi.org/10.1016/J.JNUCMAT.2012.05.048.

[15] Naveena, S. ichi Komazaki, Effect of specimen size on small punch creep behavior of high nitrogen ferritic heat-resistant steels, Mater. Sci. Eng. A. 721 (2018) 311–318. https://doi.org/10.1016/J.MSEA.2018.02.030.

[16] M.L. Saucedo-Muñoz, V. Miranda-Lopez, S. Komazaki, V.M. Lopez-Hirata, Relation of small punch creep test properties with microstructure changes for an ASTM A387 Cr–Mo steel, Mater. Sci. Eng. A. 761 (2019) 138033. https://doi.org/10.1016/J.MSEA.2019.138033.

[17] A. Chauhan, F. Bergner, A. Etienne, J. Aktaa, Y. de Carlan, C. Heintze, D. Litvinov, M. Hernandez-Mayoral, E. Oñorbe, B. Radiguet, A. Ulbricht, Microstructure

characterisation and strengthening mechanisms of oxide dispersion strengthened (ODS) Fe-9%Cr and Fe-14%Cr extruded bars, J. Nucl. Mater. 495 (2017) 6–19. https://doi.org/10.1016/J.JNUCMAT.2017.07.060.